On-site approximation for spin–orbit coupling in linear combination of atomic orbitals density functional methods

2006 J. Phys.: Condens. Matter 18 7999

(http://iopscience.iop.org/0953-8984/18/34/012)

INSTITUTE OF PHYSICS PUBLISHING JOURNAL OF PHYSICS: CONDENSED MATTER

J. Phys.: Condens. Matter **18** (2006) 7999–8013 doi:10.1088/0953-8984/18/34/012

On-site approximation for spin–orbit coupling in linear combination of atomic orbitals density functional methods

L Fernández-Seivane[1], M A Oliveira[2], S Sanvito[2] and J Ferrer[1]

[1] Departamento de Física, Universidad de Oviedo, 33007 Oviedo, Spain
[2] Department of Physics, Trinity College, Dublin 2, Republic of Ireland

Received 9 June 2006, in final form 23 July 2006
Published 11 August 2006
Online at stacks.iop.org/JPhysCM/18/7999

Abstract

We propose a computational method that drastically simplifies the inclusion of the spin–orbit interaction in density functional theory when implemented over localized basis sets. Our method is based on a well-known procedure for obtaining pseudopotentials from atomic relativistic *ab initio* calculations and on an on-site approximation for the spin–orbit matrix elements. We have implemented the technique in the SIESTA (Soler J M *et al* 2002 *J. Phys.: Condens. Matter* **14** 2745–79) code, and show that it provides accurate results for the overall band-structure and splittings of group IV and III–IV semiconductors as well as for 5d metals.

(Some figures in this article are in colour only in the electronic version)

1. Introduction

Computational methods in condensed matter physics are a powerful tool for predicting and explaining the most diverse properties of materials, nanostructures and small biological systems. Among an enormous plethora of methodologies, density functional theory (DFT) [2, 3] has become a standard for simulations at the atomic and nanometric scale. Several numerical implementations of DFT are available and the details of the algorithm usually depend on the specific applications for which the method is designed. These implementations can be categorized according to two different schemes.

The first scheme divides DFT codes depending on the basis functions used, namely plane waves or a linear combination of atomic orbitals (LCAO) (we note that some other implementations, such as LMTO [4], LAPW [5], real-space techniques [6] or wavelets [7], do not clearly fall into this classification scheme). Plane waves are typically easier to implement and the convergence is determined by a single variational parameter: the energy cutoff. In contrast, LCAO implementations are based on a tight-binding description of the chemical bond. They are more cumbersome to implement and the variational principle is controlled by a set of parameters defining the basis functions. However, these second methods are ideal for linear scaling, since a sparse Hamiltonian can be constructed by using strictly confined orbitals [8].

The second classification takes into account whether the codes simulate both core and valence electrons or only the valence electrons. In the first case, the method is regarded as *all-electron* since all the electronic degrees of freedom are treated on the same footing. This, for instance, allows one to perform fully relativistic calculations without any conceptual complication. All-electron methods are remarkably accurate but have the drawback that the calculations are usually rather intensive and only relatively small systems can be tackled. In the second case, the contribution of the core electrons is cast into pseudopotentials [9], which also can be constructed from DFT. This drastically reduces the number of electrons considered in the self-consistent simulation, and much larger systems can be investigated. A hybrid option is to use frozen core methods, such as PAW [10] and FPLO [11], which will not be discussed here.

The spin–orbit interaction is a relativistic effect whose magnitude increases with the atomic number. Consequently, it provides negligible contributions to the electronic structure of individual atoms and bulk materials made of light elements. However, it has a significant impact over the physics of heavier elements, for instance 3d ferromagnetic materials. The spin–orbit coupling can produce magnetic anisotropies of the order of 10–100 μeV for bcc and fcc Fe, Ni and Co [12], and is therefore the underlying mechanism for establishing the magnetic easy and hard axes and for controlling the shape of domain walls, together with the shape anisotropy, that is originated by dipolar magnetic interactions [13]. It is also the primary interaction responsible for most of the zero-field splitting and other properties of magnetic molecules [14].

In semiconductors, the spin–orbit interaction spin-splits the edges of the valence and conduction bands [15] and allows electrical manipulation of the spin direction [16]. This last effect is of paramount importance for the growing field of spintronics [17], which has certainly added more impetus to the inclusion of the spin–orbit interaction in the description of the electronic structure. The spin–orbit coupling determines the spin-relaxation time of electrons in ordinary semiconductors and in semiconductor heterostructures [18] and also plays an important role in the physics of diluted magnetic semiconductors [19]. Finally, it is worth mentioning that electron spin manipulation using the spin–orbit interaction was recently demonstrated in the so-called spin-Hall effect [20], which is a solid-state version of the Stern–Gerlach measurement.

It is therefore clear that the spin–orbit interaction is becoming increasingly important for a number of applications, which also require the description of rather large systems. This calls for an efficient implementation of the spin–orbit coupling within pseudopotential LCAO-based algorithms. Interestingly, most of the mainstream LCAO codes such as SIESTA [1], Onetep [21], Fireball [22], DMol^3 [23], PLATO [24] and Conquest [25] do not contain implementations of the spin–orbit interaction in their present form. In contrast, quantum chemistry packages such as Gaussian [26] or Turbomole [27] are not equipped for solid-state simulations.

Therefore we have developed a general method for including the spin–orbit interaction in conventional pseudopotential-based LCAO DFT methods. This is not computationally demanding and hence it is fully adequate for large-scale simulations. The method, although not suitable for highly accurate total energy calculations for which all electron plane-wave schemes cannot be matched, provides an excellent description of the effects of the spin–orbit coupling on the electronic structure. Here we describe our implementation within the SIESTA program [1], although the scheme is very general and could be readily implemented in any LCAO pseudopotential codes with non-collinear electron spin functionalities [28, 29].

The paper is organized as follows. We first present the details of the method, our numerical implementation and numerical tests of one- and two-centre integrals (section 3). We then demonstrate the capability of the proposed scheme with predictions for group IV and III–V semiconductors and for 5d metals (sections 4 and 5, respectively).

2. The on-site approximation

2.1. Relativistic effects in pseudopotential methods

Kleinman and Bylander have shown that the procedures for the generation of non-relativistic pseudopotentials can easily be extended to account for relativistic effects [30, 31]. This relies on solving self-consistently the all-electron Dirac equation for a single atom and in the extraction of a pseudopotential V_j, where j is now the total angular momentum $j = l \pm \frac{1}{2}$. The pseudopotential Hamiltonian can therefore be written as

$$\hat{V} = \sum_{j,m_j} |j, m_j\rangle \, V_j \, \langle j, m_j|, \tag{1}$$

and includes all relativistic corrections to order α^2, where α is the fine-structure constant and $|j, m_j\rangle$ are total angular momentum states. This expression can be recast in a form suitable for non-relativistic pseudopotential theory by expressing $|j, m_j\rangle$ in terms of a tensor product of the regular angular momentum states $|l, m\rangle$ and the eigenstates of the z component of the Pauli spin matrices [32]

$$\begin{aligned} |j = l + \tfrac{1}{2}, m_j\rangle &= \begin{pmatrix} \sqrt{\frac{l+m_j+\frac{1}{2}}{2l+1}}\, |l, m_j - \frac{1}{2}\rangle \\ \sqrt{\frac{l-m_j+\frac{1}{2}}{2l+1}}\, |l, m_j + \frac{1}{2}\rangle \end{pmatrix}, \\ |j = l - \tfrac{1}{2}, m_j\rangle &= \begin{pmatrix} \sqrt{\frac{l-m_j+\frac{1}{2}}{2l+1}}\, |l, m_j - \frac{1}{2}\rangle \\ -\sqrt{\frac{l+m_j+\frac{1}{2}}{2l+1}}\, |l, m_j + \frac{1}{2}\rangle \end{pmatrix}. \end{aligned} \tag{2}$$

Equation (1) can then be rewritten (atomic units are used throughout the article) as

$$\hat{\mathbf{V}} = \hat{\mathbf{V}}^{\mathrm{sc}} + \hat{\mathbf{V}}^{\mathrm{SO}} = \sum_{l,m} [\, \bar{V}_l \, \mathbb{1}_\sigma + \bar{V}_l^{\mathrm{SO}} \vec{L} \cdot \vec{\mathbf{S}} \,] \; |l, m\rangle\langle l, m|, \tag{3}$$

where we use bold letters to indicate 2×2 matrices, with $\mathbb{1}_\sigma$ representing the unit operator in spin space,

$$\vec{L} \cdot \vec{\mathbf{S}} = \tfrac{1}{2} \begin{pmatrix} \hat{L}_z & \hat{L}_- \\ \hat{L}_+ & -\hat{L}_z \end{pmatrix}, \tag{4}$$

and,

$$\begin{aligned} \bar{V}_l &= \frac{1}{2l+1}[(l+1)V_{l+\frac{1}{2}} + l V_{l-\frac{1}{2}}], \\ \bar{V}_l^{\mathrm{SO}} &= \frac{2}{2l+1}[V_{l+\frac{1}{2}} - V_{l-\frac{1}{2}}]. \end{aligned} \tag{5}$$

It should be stressed that the scalar part $\hat{\mathbf{V}}^{\mathrm{sc}}$ of the pseudopotential now contains not only the conventional non-relativistic pseudopotential, but also the scalar relativistic corrections.

The vectors $|l, m\rangle$, representing complex spherical harmonics, form a complete basis for the Hilbert space of the angular momentum operator $\vec{L}$. It is a useful practice in solid-state physics and quantum chemistry to replace them with real spherical harmonics $|l, M\rangle$, since the corresponding Hamiltonian is a real matrix. The change of basis is achieved by the following unitary transformation

$$\begin{aligned} |l, M\rangle &= \frac{1}{\sqrt{2}} \left(|l, m\rangle + (-1)^m \, |l, -m\rangle \right), \\ |l, \overline{M}\rangle &= \frac{1}{\sqrt{2}\,\mathrm{i}} \left(|l, m\rangle - (-1)^m \, |l, -m\rangle \right), \end{aligned} \tag{6}$$

where $M = |m|$. The case $M = 0$ is simply given by $|l, M = 0\rangle = |l, m = 0\rangle$. We note that M and $\overline{M}$ are not eigenvalues of $\bar{L}_z$, but mere labels that classify the real spherical harmonics.

The pseudopotential operator $\hat{\mathbf{V}}$ of equation (3) is now written as

$$\hat{\mathbf{V}} = \hat{\mathbf{V}}^{\mathrm{sc}} + \hat{\mathbf{V}}^{\mathrm{SO}} = \sum_{l,M} [\, \bar{V}_l \, \mathbb{1}_\sigma + \bar{V}_l^{\mathrm{SO}} \vec{L} \cdot \vec{\mathbf{S}} \,] |l, M\rangle\langle l, M|. \tag{7}$$

Finally, the Kohn–Sham Hamiltonian [3] is expressed as a sum of kinetic energy $\hat{\mathbf{T}}$, scalar relativistic $\hat{\mathbf{V}}^{\mathrm{sc}}$, spin–orbit $\hat{\mathbf{V}}^{\mathrm{SO}}$, Hartree $\hat{\mathbf{V}}^{\mathrm{H}}$ and exchange and correlation $\hat{\mathbf{V}}^{\mathrm{xc}}$ potentials:

$$\hat{\mathbf{H}} = \hat{\mathbf{T}} + \hat{\mathbf{V}}^{\mathrm{sc}} + \hat{\mathbf{V}}^{\mathrm{SO}} + \hat{\mathbf{V}}^{\mathrm{H}} + \hat{\mathbf{V}}^{\mathrm{xc}}. \tag{8}$$

This Hamiltonian is therefore a 2×2 matrix in spin space,

$$\hat{\mathbf{H}} = \begin{bmatrix} \hat{H}^{\uparrow\uparrow} & \hat{H}^{\uparrow\downarrow} \\ \hat{H}^{\downarrow\uparrow} & \hat{H}^{\downarrow\downarrow} \end{bmatrix}, \tag{9}$$

whose non-diagonal blocks arise from the exchange and correlation potential whenever the system under consideration displays a non-collinear spin, and also from the spin–orbit potential [28, 29].

2.2. Spin–orbit in LCAO schemes: the on-site approximation

LCAO methods expand the eigenstates $|\psi_n\rangle$ of the non-collinear Kohn–Sham Hamiltonian over a set of localized orbitals $|\phi_i\rangle$,

$$|\psi_n\rangle = \sum_i \begin{pmatrix} c_{n,i}^{\uparrow} \\ c_{n,i}^{\downarrow} \end{pmatrix} |\phi_i\rangle \tag{10}$$

where i is a collective index for all the symbols required to describe uniquely a given orbital

$$|\phi_i\rangle = |\phi_{n_i,l_i,M_i}\rangle = |R_{n_i,l_i}\rangle \otimes |l_i, M_i\rangle. \tag{11}$$

Here both the radial and angular part of the wavefunction $\phi_i(\vec{r} - \vec{d}_i) = \langle \vec{r} \,|\phi_i\rangle$ is centred at the position $\vec{d}_i$. Note that n_i does not necessarily describe the principle quantum number only, but generally labels a set of radial functions associated with the angular momentum l_i according to the multiple zetas scheme [33].

The Kohn–Sham equation, $\hat{H}\,|\psi_n\rangle = E_n\,|\psi_n\rangle$, is then projected onto such an orbital basis set as

$$\begin{bmatrix} H_{ij}^{\uparrow\uparrow} - E_n S_{ij} & H_{ij}^{\uparrow\downarrow} \\ H_{ij}^{\downarrow\uparrow} & H_{ij}^{\downarrow\downarrow} - E_n S_{ij} \end{bmatrix} \begin{bmatrix} c_{n,j}^{\uparrow} \\ c_{n,j}^{\downarrow} \end{bmatrix} = 0, \tag{12}$$

where $H_{ij}^{\sigma\sigma'} = \langle \phi_i | \hat{H}^{\sigma\sigma'} | \phi_j \rangle$ and $S_{ij} = \langle \phi_i | \phi_j \rangle$ are the matrix elements of the Hamiltonian and overlap matrix, respectively.

The spin–orbit term can then be calculated as

$$\mathbf{V}_{ij}^{\mathrm{SO}} = \langle \phi_i | \hat{\mathbf{V}}^{\mathrm{SO}} | \phi_j \rangle = \sum_{k,l_k,M_k} \langle \phi_i | \bar{V}_{l_k}^{\mathrm{SO}} \vec{L} \cdot \vec{S} \, |l_k, M_k\rangle \, \langle l_k, M_k | \phi_j \rangle, \tag{13}$$

where index k indicates the atom on which the potential is centred, $\bar{V}_{l_k}^{\mathrm{SO}} = \bar{V}_l^{\mathrm{SO}}(\vec{r} - \vec{d}_k)$ and $|l_k, M_k\rangle$ is the spherical harmonic centred at the same atomic position $\vec{d}_k$. Equation (13) involves a considerable number of three-centre integrals. Inclusion of the spin–orbit interaction is therfore, in the LCAO approach, computationally intensive, if straightforward. One possibility of reducing the computational effort is to construct fully non-local pseudopotentials [34]. We note, however, that the radial part of the spin–orbit pseudopotentials, $\bar{V}_l^{\mathrm{SO}}$, is very short-ranged, resulting in matrix elements that decay quickly with the distance among the three centres. Thus we consider only matrix elements where

the three components, both orbitals and the pseudopotential, reside on the same atom, and discard all the rest. This approximation simplifies the matrix elements of equation (13) to one-centre integrals and drastically reduces the computational effort needed to account for spin–orbit effects. Then our approximated matrix elements are

$$\mathbf{V}_{ij}^{\mathrm{SO}} = \tfrac{1}{2} \sum_{k,l_k>0,M_k} \langle R_{n_i,l_i}|\bar{V}_{l_k}^{\mathrm{SO}}|R_{n_j,l_j}\rangle \, \langle l_i, M_i| \begin{pmatrix} \hat{L}_z & \hat{L}_- \\ \hat{L}_+ & -\hat{L}_z \end{pmatrix} |l_k, M_k\rangle \, \langle l_k, M_k|l_j, M_j\rangle$$
$$\approx \tfrac{1}{2} \, \langle R_{n_i,l_i}|\bar{V}_{l_i}^{\mathrm{SO}}|R_{n_j,l_i}\rangle \, \langle l_i, M_i| \begin{pmatrix} \hat{L}_z & \hat{L}_- \\ \hat{L}_+ & -\hat{L}_z \end{pmatrix} |l_i, M_j\rangle \, \delta_{l_i,l_j}, \tag{14}$$

since the $\hat{L}_\alpha$ operators leave each l_i subspace invariant. The angular part of these on-site matrix elements can be calculated analytically:

$$\langle l_i, M_i|\hat{L}_\pm|l_i, M_j\rangle = \tfrac{1}{2}\left\{A_{M_j}^{+}\left(\delta_{M_i,M_j+1} \pm \mathrm{i}\,\delta_{M_i,\overline{M_j+1}}\right) - A_{M_j}^{-}\left(\delta_{M_i,M_j-1} \mp \mathrm{i}\,\delta_{M_i,\overline{M_j-1}}\right)\right\},$$
$$\langle l_i, M_i|\hat{L}_\pm|l_i, \overline{M}_j\rangle = \tfrac{1}{2}\left\{A_{M_j}^{+}\left(\delta_{M_i,M_j+1} \pm \mathrm{i}\,\delta_{M_i,\overline{M_j+1}}\right) + A_{M_j}^{-}\left(\delta_{M_i,M_j-1} \mp \mathrm{i}\,\delta_{M_i,\overline{M_j+1}}\right)\right\},$$
$$\langle l_i, M_i|\hat{L}_z|l_i, M_j\rangle = \mathrm{i}M_j\,\delta_{M_i,\overline{M}_j},$$
$$\langle l_i, M_i|\hat{L}_\pm|l_i, 0\rangle = \pm\frac{A_0^{\pm}}{\sqrt{2}}\left(\delta_{M_i,1} \pm \mathrm{i}\,\delta_{M_i,\overline{1}}\right) \tag{15}$$

where $A_{M_j}^{\pm} = \sqrt{l_i(l_i+1) - M_j(M_j \pm 1)}$ are Clebsh–Gordan coefficients.

Some useful symmetries of the matrix elements of the Hamiltonian and of its spin–orbit part should also be highlighted. Since the Hamiltonian is hermitian, the matrix elements satisfy the relation

$$H_{ij}^{\sigma\sigma'} = (H_{ji}^{\sigma'\sigma})^*. \tag{16}$$

Moreover, it is also easy to show that all the terms in the Hamiltonian satisfy a spin box hermiticity, i.e.

$$H_{ij}^{\sigma\sigma'} = (H_{ij}^{\sigma'\sigma})^*, \tag{17}$$

except for the spin–orbit contribution, which is spin box anti-Hermitian:

$$H_{ij}^{\sigma\sigma'} = -(H_{ij}^{\sigma'\sigma})^*. \tag{18}$$

This property has important consequences for the calculation of the total energy.

2.3. Density matrix and total energy

The charge density can also be written in terms of the LCAO basis as

$$\mathbf{n}(\vec{r}) = \sum_n \; f_n \; \psi_n(\vec{r}) \; \psi_n(\vec{r})^\dagger = \sum_{i,j} \phi_i(\vec{r} - \vec{d}_i) \, \phi_j^*(\vec{r} - \vec{d}_j) \; \rho_{ij} \tag{19}$$

where f_n represents the occupation of the Kohn–Sham eigenstate $\psi_n(\vec{r}\,)$ and ρ_{ij} is a 2×2 matrix containing the products of wavefunction coefficients, whose components are

$$\rho_{ij}^{\sigma\sigma'} = \sum_n \; f_n \; c_{n,i}^{\sigma} \, c_{n,j}^{\sigma'*}. \tag{20}$$

The electronic contribution to the total energy may be expressed as a sum of a band-structure (BS) contribution plus double-counting corrections. The BS contribution can be written in the LCAO basis as

$$E_e^{BS} = \sum_n f_n \; \langle\psi_n|\hat{\mathbf{H}}|\psi_n\rangle = \sum_{i,j,\sigma,\sigma'} H_{ij}^{\sigma\sigma'} \rho_{ji}^{\sigma'\sigma}, \tag{21}$$

which may also be expressed as

$$\sum_{ij}\left\{H_{ij}^{\uparrow\uparrow}\,\rho_{ji}^{\uparrow\uparrow}+H_{ij}^{\downarrow\downarrow}\,\rho_{ji}^{\downarrow\downarrow}+2\ \mathrm{Re}\left[(V_{ij}^{\mathrm{xc}\uparrow\downarrow}-V_{ij}^{\mathrm{SO}\uparrow\downarrow})\,(\rho_{ji}^{\uparrow\downarrow})^{*}\right]\right\}, \tag{22}$$

where we have isolated the non-diagonal contributions in spin space. These arise only from the spin–orbit interaction and from the exchange and correlation potential whenever spin non-collinearity is present. The spin–orbit contribution to the total energy is therefore

$$E^{\mathrm{SO}}=\mathrm{Tr}\sum_{i,j}\mathbf{V}_{ij}^{\mathrm{SO}}\,\rho_{ji}, \tag{23}$$

since there are no double-counting terms. The Trace is over the spin degrees of freedom.

2.4. Forces and stresses

One important consequence of the on-site approximation is that spin–orbit does not give rise to an explicit contribution to forces and stresses, even though an implicit contribution due to the modification of the self-consistent wavefunction is always present. According to Hellmann–Feynman theorem [35], the spin–orbit contribution to the forces excerpted upon an atom centred at position $\vec{d}_k$ is obtained by simply differentiating the energy with respect to the atomic coordinates of the atom,

$$-\vec{F}_k^{\mathrm{SO}}=\vec{\nabla}_k E^{\mathrm{SO}}=\mathrm{Tr}\sum_{i,j}\left\{\left[\vec{\nabla}_k\hat{\mathrm{V}}_{ij}^{\mathrm{SO}}\right]\rho_{ji}+\mathbf{V}_{ij}^{\mathrm{SO}}\left[\vec{\nabla}_k\hat{\rho}_{ji}\right]\right\}, \tag{24}$$

where both the i and j orbitals are centred at the same atomic position $\vec{d}_k$ and $\vec{\nabla}_k=\vec{\nabla}_{\vec{d}_k}$, and Tr means trace over spins. However, both contributions to the spin–orbit forces in equation (24) vanish. The first one is identically zero, since the one-centre integrals do not depend on the atomic position,

$$\nabla_k\langle R_{n_i,l_i}|\bar{V}_{l_k}^{\mathrm{SO}}|R_{n_j,l_j}\rangle\equiv 0. \tag{25}$$

The second term may be rewritten as

$$-\sum_{ij}\left(\mathcal{E}_{ij}^{\mathrm{SO},\uparrow\uparrow}+\mathcal{E}_{ij}^{\mathrm{SO},\downarrow\downarrow}\right)\vec{\nabla}_k S_{ji}, \tag{26}$$

where $\mathcal{E}_{ij}^{\mathrm{SO},\sigma\sigma'}$ are the components of the spin–orbit contribution to the energy-density matrix

$$\mathcal{E}_{ij}^{\mathrm{SO}}=\tfrac{1}{2}\sum_{l,m}(S_{il}^{-1}\,\mathbf{V}_{lm}^{\mathrm{SO}}\,\rho_{mj}+\rho_{il}\,\mathbf{V}_{lm}^{\mathrm{SO}}\,S_{mj}^{-1}). \tag{27}$$

However, since $\mathcal{E}^{\mathrm{SO}}$ is antisymmetric with respect to the orbital indices, in contrast to the overlap matrix, which is symmetric, the second term vanishes as well.

In a similar way, one can demonstrate that the spin–orbit interaction in the on-site approximation does not introduce any additional contribution to the stress.

3. Numerical tests on one- and two-centre integrals

The validity of the on-site approximation relies on the fact that two- and three-centre integrals are much smaller than the one-centre integrals, which are kept in the simulation. Among those two- and three-centre matrix elements, the two-centre integrals

$$\mathbf{V}_{ij}^{2c}(\vec{R})=\langle\phi_i(\vec{R})\,|\bar{V}_{l_j}^{\mathrm{SO}}(0)\,\vec{L}(0)\cdot\vec{\mathbf{S}}(0)\,|\phi_j(0)\rangle, \tag{28}$$

are expected to have the largest absolute value. An excellent test consists of calculating these matrix elements for a given material along the direction that joins one atom to its nearest

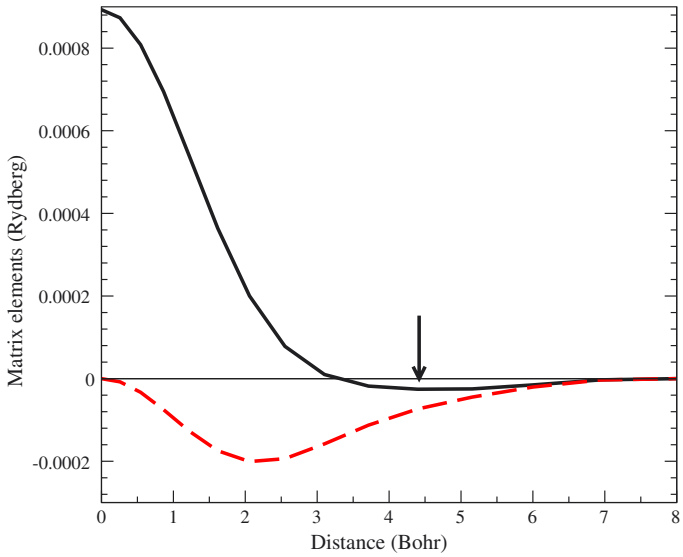

Figure 1. Two-centre integrals $\mathbf{V}^z_{y-x}(R)$ and $\mathbf{V}^z_{z-x}(R)$ (solid and dashed lines, respectively) for silicon along the (111) direction, as a function of the distance R between the two centres. The arrow indicates the distance of the nearest-neighbour atoms.

neighbours, as a function of the distance R between the two centres. Then, $R = 0$ provides the on-site matrix elements, while, if R equals the nearest-neighbour distance, the calculation describes the desired two-centre integrals. We have performed such a test for a representative semiconductor, Si, and a representative 5d metal, Pt.

For silicon, the valence electrons include s- and p-orbitals only and therefore we consider the following matrix elements:

$$\begin{aligned}\mathbf{V}^z_{y-x}(R) &= \langle\phi_{p_y}(R)\,|\bar{V}^{\mathrm{SO}}_p(0)\,L_z(0)\,|\phi_{p_x}(0)\rangle,\\ \mathbf{V}^z_{z-x}(R) &= \langle\phi_{p_z}(R)\,|\bar{V}^{\mathrm{SO}}_p(0)\,L_z(0)\,|\phi_{p_x}(0)\rangle.\end{aligned} \tag{29}$$

For $R = 0$, the first of these matrix elements reduces to the on-site integral $\mathbf{V}^z_{y-x}(0)$, while the second is zero by symmetry. Figure 1 shows the matrix elements as a function of R along the direction (111). The matrix elements, evaluated at the nearest-neighbour distance, are considerably smaller than the on-site integral, with the $\mathbf{V}(R)/\mathbf{V}(0)$ ratio being $\sim$0.03 and $\sim$0.08, respectively, for $y - x$ and $z - x$.

In the case of Pt, we have considered not only the 5d but also the 6p orbitals. Platinum crystallizes with an fcc structure and a nearest-neighbour distance of 5.4 au. We compute the same p-matrix elements as for silicon, as well as the two following d integrals:

$$\begin{aligned}\mathbf{V}^z_{x^2y^2-xy}(R) &= \langle\phi_{x^2-y^2}(R)\,|\bar{V}^{\mathrm{SO}}_d(0)\,L_z(0)\,|\phi_{xy}(0)\rangle,\\ \mathbf{V}^z_{z^2-xz}(R) &= \langle\phi_{3z^2-r^2}(R)\,|\bar{V}^{\mathrm{SO}}_d(0)\,L_z(0)\,|\phi_{xz}(0)\rangle.\end{aligned} \tag{30}$$

Figure 2 shows these matrix elements as a function of R. For the d-type matrix elements (figure 2(a)), the decay with the distance between the centres is rather dramatic and the two-centre matrix elements are about 10^{-4} times smaller than the on-site integrals. The case of the p-integrals (figure 2(b)) is similar to that of Si with a $\mathbf{V}(R)/\mathbf{V}(0)$ ratio of $\sim$0.08. For the specific case of Pt, however, these p-integrals are expected to contribute little to any physical quantities, since they correspond to unoccupied states.

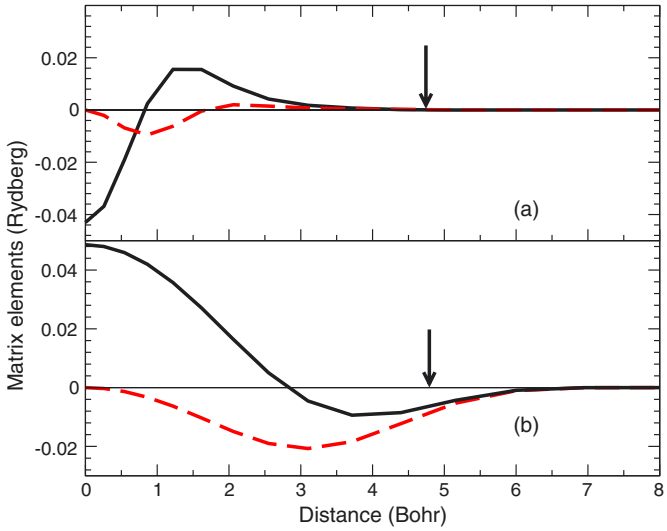

Figure 2. (a) Two-centre integral $\mathbf{V}^{z}_{x^2-y^2-xy}(R)$ and $\mathbf{V}^{z}_{z^2-xz}(R)$ (solid and dashed lines, respectively) and (b) $\mathbf{V}^{z}_{y-x}(R)$ and $\mathbf{V}^{z}_{z-x}(R)$ (also, solid and dashed lines, respectively) for platinum along the (110) direction as a function of the distance R between the two centres. The arrow indicates the distance of the nearest-neighbour atoms.

The same tests for other materials give similar results. We therefore conclude that the on-site approximation provides accurate results for heavy transition metals and good quantitative estimates for semiconductors. For the latter, we estimate an error due to the neglecting of high-centre integrals not larger than 10%, and on average of the order of 3–6%.

4. Spin–orbit in group IV and III–V semiconductors

We have thus demonstrated that, in general, our on-site approximation simplifies the inclusion of spin–orbit effects in LCAO DFT codes. We have thus implemented the method in SIESTA, a LCAO code able to simulate non-collinear arrangements of spins [1, 29], that in addition reads relativistically generated pseudopotentials in the form required by equation (1).

The numerical implementation is rather simple, since the spin–orbit contribution to the Hamiltonian does not depend on the electron charge density and therefore does not need to be updated during the self-consistent procedure. This drastically reduces the computational overheads, which are almost identical to those of a standard non-collinear spin-polarized calculation. Here we present a series of test cases for the band-structures of group IV and III–V semiconductors, obtained with the local spin density approximation and norm-conserving relativistic pseudopotentials. Special care was taken in the generation of the pseudopotentials and of the basis sets and in the choice of the parameters that control the numerical accuracy of real- and reciprocal-space integrals [1]. In particular, the basis set was highly optimized, following the scheme proposed in [36, 37], from which we have borrowed our notation for multiple zeta basis sets SZ, SZP, DZ, DZP, TZ, TZP, TZDP, TZTP, and TZTPF.

The introduction of the spin–orbit interaction lifts specific degeneracies in the band-structure of a material. In particular, for diamond and zincblende semiconductors the six-fold degenerate valence band Γ^{v}_{15} at Γ splits into two. The first is four-fold degenerate Γ^{v}_{8} (the heavy- and light-hole bands), and the second is only two-fold degenerate Γ^{v}_{7} (the spin-split-off band).

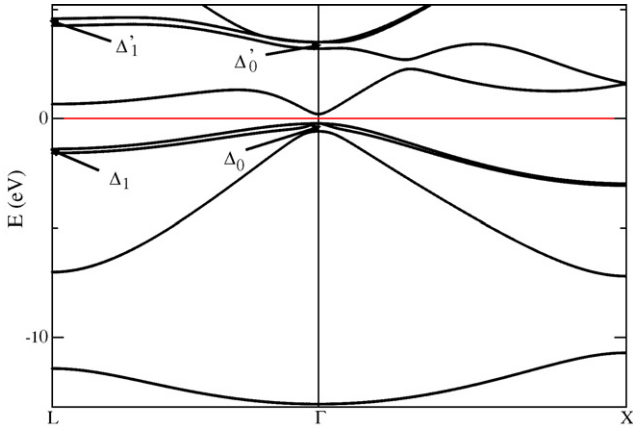

Figure 3. Band-structure of GaAs calculated with the on-site approximation to the spin–orbit interaction.

Table 1. Spin–orbit energy splittings of bulk Si calculated for increasingly complete basis sets. E_T is the total energy, Δ_0, Δ_0', Δ_1 and Δ_1' are the splittings as defined in the text. REF corresponds to the reference values, experimental whenever possible, as described in the literature [38].

Basis	E_T (eV)	Δ_0 (eV)	Δ_0' (eV)	Δ_1 (eV)	Δ_1' (eV)
SZ	−214.8	0.051	0.025	—	—
DZ	−215.0	0.068	0.157	0.027	0.105
TZ	−215.2	0.068	0.002	0.023	0.078
SZP	−215.8	0.042	0.787	0.024	0.032
DZP	−216.0	0.044	0.647	0.024	0.047
TZP	−216.0	0.045	0.696	0.025	0.050
TZDP	−216.0	0.045	0.604	0.026	0.043
TZTP	−216.0	0.045	0.593	0.026	0.044
TZTPF	−216.1	0.044	0.615	0.025	0.030
REF	—	0.044	0.04	0.02	0.03

This energy splitting Δ_0 ($\Gamma_{15}^v \rightarrow \Gamma_8^v, \Gamma_7^v$) is the hallmark of the effects of spin–orbit interaction in the band-structure of these materials. Other commonly measured energy splittings are called Δ_0' ($\Gamma_{15}^c \rightarrow \Gamma_8^c, \Gamma_7^c$), Δ_1 ($L_3^v \rightarrow L_{4,5}^v, L_6^v$) and Δ_1' ($L_3^c \rightarrow L_{4,5}^c, L_6^c$).

In figure 3 we show the band-structure of the canonical III–V semiconductor, GaAs. The figure also defines graphically the energy splittings described in the previous paragraph. We note first that the band-structure closely resembles that obtained with other methodologies, and also agrees rather well with the experimental data [38], except for the characteristic local density approximation (LDA) underestimation of the semiconductor gap, which is further reduced because of the spin–orbit energy splitting. Therefore, in all the tests that follow, we have avoided narrow-gap semiconductors, which are usually predicted by LDA to be metals [39].

4.1. Band-structure of Si

The spin–orbit energy splittings of silicon at the high-symmetry points of the diamond lattice are presented in table 1 and figure 4 for increasingly complete basis sets.

Our results are in extremely good agreement with the theoretical and experimental data available in the literature [38]. We note that a DZP basis set, which is usually assumed to

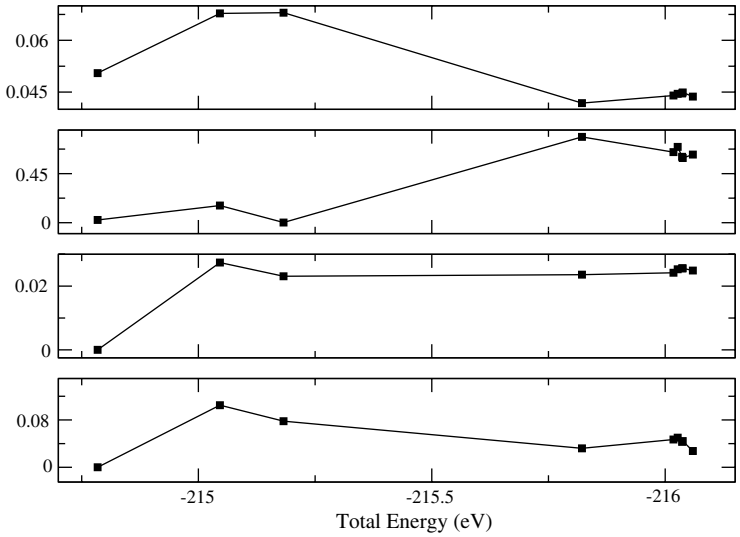

Figure 4. Convergence of the spin–orbit energy splittings of bulk Si with the size of the basis set. From top to bottom panels, we present respectively Δ_0, Δ_0', Δ_1 and Δ_1' as functions of the total energy associated with each set. The points correspond to SZ, DZ, TZ, SZP, DZP, TZP, TZDP, TZTP and TZTPF, respectively.

be the minimal basis needed to obtain reasonably converged results, already provides accurate predictions for the energy splittings. The Δ_0' split is somehow an anomaly, and in general we find that the splittings of the conduction bands are not as well described as those of the valence bands.

We note that Kohn–Sham eigenvalues should not be associated with single particle excitation energies, since the former are simply the Lagrangian multipliers leading to the Kohn–Sham equations. This is valid for both the valence and the conduction bands. However, it is commonly accepted that DFT band-structures are a good first approximation to single particle energies of occupied states. The conduction bands are somehow different, since such states do not contribute to either the total energy or the density matrix, and therefore are irrelevant in DFT. For this reason, a stark disagreement in the conduction band splitting should not be surprising.

It is also important to note that the basis where the radial component varies sharply around the origin should be avoided. These, in fact, are difficult to integrate in the range where the spin–orbit pseudopotential is appreciable and brings considerable numerical instability to the evaluation of the matrix elements, or require an insanely fine mesh.

Finally, we have calculated the Si bulk parameters for different basis sets in order to check that the inclusion of spin–orbit interaction does not change significantly the LDA results. A summary of all the computed structural parameters is presented in table 2.

4.2. III–V semiconductors

We have further tested our method by calculating the various energy splittings of several group IV and III–V semiconductors such as Ge, GaAs, AlAs and AlSb, i.e. of those with a reasonably large bandgap. For all of them we have found again that a DZP basis set provides essentially converged results. This is demonstrated in table 3 where we show that the splittings calculated

Table 2. Structural parameters of bulk Si for several basis sets. a is the lattice parameter, BM the bulk modulus and E_c the cohesive energy. PW refers to a 50 Ryd cutoff plane-wave calculation [1]. LAPW corresponds to an all-electron linear-augmented-plane-wave calculation [40] and EXP to the experimental values [41].

Basis	a (Å)	BM (GPa)	E_c (eV)
DZP	5.392	98.2	5.480
TZP	5.389	98.8	5.485
TZTP	5.388	98.2	5.491
PW	5.384	95.9	5.369
LAPW	5.41	96	5.28
EXP	5.43	98.8	4.64

Table 3. Spin splittings for several III–V semiconductors as calculated with a DZP basis set. REF correspond to reference values, experimental whenever possible, as described in the literature [42, 38, 43].

Material	Δ_0 (eV)	Δ_0' (eV)	Δ_1 (eV)	Δ_1' (eV)
Ge	0.2959	0.3783	0.1545	0.356
REF [42]	0.287	0.200	0.184	0.266
GaAs	0.3573	0.3006	0.1857	0.319
REF [38]	0.34	0.26	0.23	0.11
AlAs	0.3073	0.0762	0.1636	0.118
REF [43]	0.28	0.04	0.20	—
AlSb	0.6847	0.1752	0.3440	0.307
REF [38]	0.75	0.1	0.4	0.09

with a DZP basis agree rather well with other theoretical estimates and with experimental values. Also in this case Δ_0' is the exception for the same reasons explained before.

5. 5d metals: Au and Pt

Since the spin–orbit interaction is a relativistic effect, it is expected to increase with the atomic number. Therefore, metals from the fifth row of the periodic table are an ideal test ground for our method. Among those, gold and platinum are especially good candidates, since the first is a closed-d shell noble metal while the d-bands of the second have considerable weight at the Fermi energy. Moreover, a number of *ab initio* spin–orbit calculations are available [44] which demonstrate that the spin–orbit interaction is essential for the correct description of their band-structures. To simulate these two materials, we have again used the LDA approximation for the exchange and correlation potentials, and constructed an optimized set consisting of two atomic wavefunctions in each of the s-, p- and d-channels.

In figures 5 and 6 we present the band-structures of Pt and Au, calculated at the theoretical lattice constant, with and without taking into account the spin–orbit coupling. The figures show that s-bands are not modified by spin–orbit coupling, while p- and d-bands suffer strong modifications, especially whenever two bands cross each other. Moreover, we find that the spin–orbit interaction lifts degeneracies at the band crossings, as expected.

In table 4 we summarize the bulk lattice constant and the energy of some selected bands at the Γ point, which we define graphically in figure 5. These energies are in good agreement with other much more expensive methods, like plane-wave pseudopotential (PWSCF) [44] and relativistic full-potential Korringa–Kohn–Rostoker (KKR) [45] methods or augmented

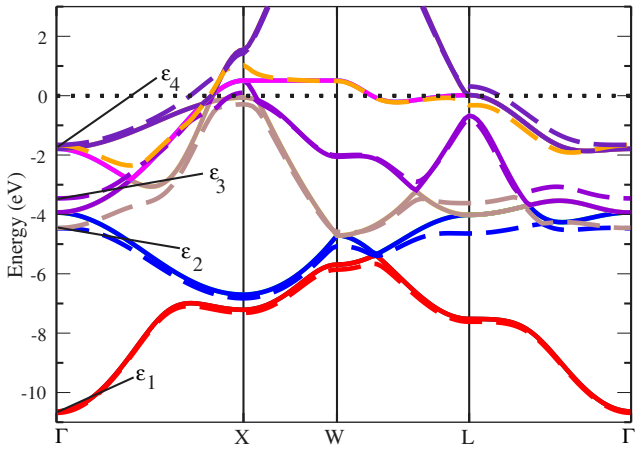

Figure 5. Band-structure of platinum obtained at the theoretical equilibrium lattice constant. The dashed line is for a spin–orbit calculation, while the solid line is obtained when the spin–orbit coupling is not included. The figure also provides a graphical definition of the energies at the Γ point, ε_i, of the bands that are closest to the Fermi energy.

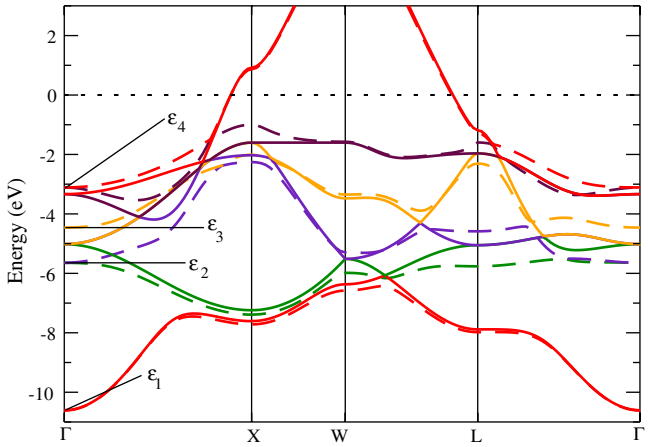

Figure 6. Band-structure of gold obtained at the equilibrium theoretical lattice constant. The dashed line is for a spin–orbit calculation, while the solid line is obtained when the spin–orbit coupling is not included. The figure also provides a graphical definition of the energies at the Γ point, ε_i, of the bands that are closest to the Fermi energy.

plane-wave (APW) approaches for solving the Dirac equation [46]. We note that the differences range over the order of only a few per cent.

6. Conclusion

We have presented a simple and effective method for including the spin–orbit interaction in standard LCAO DFT calculations that is based on relativistic norm-conserving pseudopotentials and on an on-site approximation to the spin–orbit matrix elements. The method is computationally undemanding and extremely simple to implement in standard LCAO DFT codes, such as SIESTA. Importantly, the on-site approximation does not introduce

Table 4. Lattice constant and energy ε_i of selected bands at the Γ point obtained with the use of the approximation presented in this paper (SIESTA + on-site), and with PWSCF [44], KKR [45] and APW [46] methods. The definition of the energies ε_i is provided in figures 3 and 4.

Pt	SIESTA + on-site	PWSCF	KKR	APW
a_0 (Bohr)	7.45	7.40	7.36	7.414
ε_1 (eV)	−10.53	−10.45	−10.56	−10.35
ε_2 (eV)	−4.38	−4.38	−4.48	−4.24
ε_3 (eV)	−3.38	−3.39	−3.47	−3.28
ε_4 (eV)	−1.62	−1.53	−1.65	−1.48
Au	SIESTA + on-site	PWSCF	KKR	APW
a_0 (Bohr)	7.61	7.64	7.637	7.638
ε_1 (eV)	−10.613	−10.18	−10.23	−9.95
ε_2 (eV)	−5.645	−5.43	−5.41	−5.32
ε_3 (eV)	−4.460	−4.23	−4.23	−4.14
ε_4 (eV)	−3.111	−2.97	3.04	2.96

additional contributions to both forces and stress. We have then presented a series of tests for group IV and III–V semiconductors and for 5d metals. The overall structural parameters do not change with respect to standard non-relativistic LDA calculations, and are in general good agreement with reference data. The spin–orbit splittings of the band-structures are also in good agreement with those obtained with more computationally intensive DFT methods.

The good results obtained for the electronic structures and structural parameters make our method very attractive for large-scale simulations where spin–orbit coupling is relevant. This is the case, for instance, for semiconductors heterostructures and quantum-transport calculations [47] where spin-mixing effects are important.

Acknowledgments

We wish to thank D Sánchez-Portal, V García-Suárez, P Ordejón and J Soler for useful discussions. LFS acknowledges the support of FICYT through grant BP04-087. The research presented in this paper has been performed under the financial support of the Science Foundation of Ireland (SFI02/IN1/I175) and the Spanish Ministerio de Educación y Ciencia through project BFM2003-03156. Travel was supported by Enterprise Ireland (IC 2004 84).

References

[1] Soler J M, Artacho E, Gale J D, Junquera A G J, Ordejón P and Sánchez-Portal D 2002 The SIESTA method for *ab initio* order-N materials simulations *J. Phys.: Condens. Matter* **14** 2745–79
[2] Hohenberg P and Kohn W 1964 Inhomogeneous electron gas *Phys. Rev.* **136** B864–71
[3] Kohn W and Sham L J 1965 Self-consistent equations including exchange and correlation effects *Phys. Rev.* **140** A1133–8
[4] Andersen O K 1975 Linear methods in band theory *Phys. Rev.* B **12** 3060–83
[5] Blaha P, Schwarz K and Sorantin P 1990 Full-potential, linearized augmented plane wave programs for crystalline systems *Comput. Phys. Commun.* **59** 399–415
[6] Beck T L 2000 Real-space mesh techniques in density-functional theory *Rev. Mod. Phys.* **72** 1041–80
[7] Arias T A 1999 Multiresolution analysis of electronic structure: semicardinal and wavelet bases *Rev. Mod. Phys.* **71** 267–311
[8] Goedecker S 1999 Linear scaling electronic structure methods *Rev. Mod. Phys.* **71** 1085–123, available from: http://link.aps.org/abstract/RMP/v71/p1085

[9] Martin R M 2004 *Electronic Structure: Basic Theory and Practical Methods* (Cambridge: Cambridge University Press)

[10] Kresse G and Joubert D 1999 From ultrasoft pseudopotentials to the projector augmented-wave method *Phys. Rev.* B **59** 1758–75

[11] Koepernik K and Eschrig H 1999 Full-potential nonorthogonal local-orbital minimum-basis band-structure scheme *Phys. Rev.* B **59** 1743–57

[12] Burkert T, Eriksson O, James P, Simak S I, Johansson B and Nordstrom L 2004 Calculation of uniaxial magnetic anisotropy energy of tetragonal and trigonal Fe, Co, and Ni *Phys. Rev.* B **69** 104426, available from: http://link.aps.org/abstract/PRB/v69/e104426

[13] Bruno P 2004 *Electronic Structure: Basic Theory and Practical Methods* (Cambridge: Cambridge University Press)

[14] Gatteschi D and Sessoli R 2003 Quantum tunneling of magnetization and related phenomena in molecular materials *Angew. Chem. Int. Edn* **42** 268–97, available from: http://dx.doi.org/10.1002/anie.200390099

[15] Yu P Y and Cardona M 2005 *Fundamentals of Semiconductors: Physics and Materials Properties* (Berlin: Springer)

[16] Datta S and Das B 1990 Electronic analog of the electro-optic modulator *Appl. Phys. Lett.* **56** 665–7, available from: http://link.aip.org/link/?APL/56/665/1

[17] Wolf S A *et al* 2001 Spintronics: a spin-based electronics vision for the future *Science* **294** 1488–95, available from: http://www.sciencemag.org/cgi/content/abstract/294/5546/1488

[18] Kikkawa J M and Awschalom D D 1999 Lateral drag of spin coherence in gallium arsenide *Nature* **397** 139–41

[19] Sanvito S, Theurich G and Hill N A 2002 Density functional calculations for III–V diluted ferromagnetic semiconductors: a review *J. Supercond.* **15** 85–104, available from: http://dx.doi.org/10.1023/A:1014083312066

[20] Kato Y K, Myers R C, Gossard A C and Awschalom D D 2004 Observation of the spin Hall effect in semiconductors *Science* **306** 1910–3, available from: http://www.sciencemag.org/cgi/content/abstract/306/5703/1910

[21] Skylaris C K, Haynes P D, Mostofi A A and Payne M C 2005 Using ONETEP for accurate and efficient $\mathcal{O}(N)$ density functional calculations *J. Phys.: Condens. Matter* **17** 5757–69, available from: http://stacks.iop.org/0953-8984/17/5757

[22] Shellman S D, Lewis J P, Glaesemann K R, Sikorski K and Voth G A 2003 Massively parallel linear-scaling algorithm in an *ab initio* local-orbital total-energy method *J. Comput. Phys.* **188** 1–15

[23] Delley B 1990 An all-electron numerical method for solving the local density functional for polyatomic molecules *J. Chem. Phys.* **92** 508–17, available from: http://link.aip.org/link/?JCP/92/508/1

[24] Kenny S D, Horsfield A P and Fujitani H 2000 Transferable atomic-type orbital basis sets for solids *Phys. Rev.* B **62** 4899–905

[25] Bowler D R, Choudhury R, Gillan M J and Miyazaki T 2006 Recent progress with large-scale *ab initio* calculations: the CONQUEST code *Phys. Status Solidi* b **243** 989–1000, available from: http://dx.doi.org/10.1002/pssb.200541386

[26] Frisch M J *et al* 2004 *Gaussian 03, Revision C.02* (Wallingford, CT: Gaussian, Inc.)

[27] Ahlrichs R, Bär M, Häser M, Hom H and Kölmel C 1989 Electronic structure calculations on workstation computers: the program system turbomole *Chem. Phys. Lett.* **162** 165–9, available from: http://dx.doi.org/10.1016/0009-2614(89)85118-8

[28] Sandratskii L M 1998 Noncollinear magnetism in itinerant-electron systems: theory and applications *Adv. Phys.* **47** 91–160, available from: http://dx.doi.org/10.1080/000187398243573

[29] García-Suárez V M, Newman C M, Lambert C J, Pruneda J M and Ferrer J 2004 Optimized basis sets for the collinear and non-collinear phases of iron *J. Phys.: Condens. Matter* **16** 5453–9, available from: http://stacks.iop.org/0953-8984/16/5453

[30] Kleinman L 1980 Relativistic norm-conserving pseudopotential *Phys. Rev.* B **21** 2630–1

[31] Bachelet G B and Schüter M 1982 Relativistic norm-conserving pseudopotentials *Phys. Rev.* B **25** 2103–8

[32] Schwabl F 2002 *Quantum Mechanics* (Berlin: Springer)

[33] Sankey O F and Niklewski D J 1989 *Ab initio* multicenter tight-binding model for molecular-dynamics simulations and other applications in covalent systems *Phys. Rev.* B **40** 3979–95, available from: http://link.aps.org/abstract/PRB/v40/p3979

[34] Kleinman L and Bylander D M 1982 Efficacious form for model pseudopotentials *Phys. Rev. Lett.* **48** 1425–8, available from: http://link.aps.org/abstract/PRL/v48/p1425

[35] Feynman R P 1939 Forces in molecules *Phys. Rev.* **56** 340–3, available from: http://link.aip.org/link/PR/56/340/1

[36] Junquera J, Óscar Paz D S P and Artacho E 2001 Numerical atomic orbitals for linear-scaling calculations *Phys. Rev.* B **64** 235111
[37] Anglada E, Soler J M, Junquera J and Artacho E 2002 Systematic generation of finite-range atomic basis sets for linear-scaling calculations *Phys. Rev.* B **66** 205101
[38] Wepfer G G, Collins T C and Euwema R N 1971 Calculated spin–orbit splittings of some group IV, III–V, and II–VI semiconductors *Phys. Rev.* B **4** 1296–306, available from: http://link.aps.org/abstract/PRB/v4/p1296
[39] Surh M P, Li M F and Louie S G 1991 Spin–orbit splitting of GaAs and InSb bands near Γ *Phys. Rev.* B **43** 4286–94
[40] Filippi C, Singh D J and Umrigar C J 1994 All-electron local-density and generalized-gradient calculations of the structural properties of semiconductors *Phys. Rev.* B **50** 14947–51
[41] Kittel C 1986 *Introduction to Solid State Physics* (New York: Wiley)
[42] Aspnes D E 1975 Schottky-barrier electroreflectance of Ge: nondegenerate and orbitally degenerate critical points *Phys. Rev.* B **12** 2297–310, available from: http://link.aps.org/abstract/PRB/v12/p2297
[43] Mäder K A and Zunger A 1994 Empirical atomic pseudopotentials for AlAs/GaAs superlattices, alloys, and nanostructures *Phys. Rev.* B **50** 17393–405
[44] Corso A D and Conte A M 2005 Spin–orbit coupling with ultrasoft pseudopotentials: application to Au and Pt *Phys. Rev.* B **71** 115106, available from: http://link.aps.org/abstract/PRB/v71/e115106
[45] Theileis V and Bross H 2000 Relativistic modified augmented plane wave method and its application to the electronic structure of gold and platinum *Phys. Rev.* B **62** 13338–46, available from: http://link.aps.org/abstract/PRB/v62/p13338
[46] der Kellen S B and Freeman A J 1996 Self-consistent relativistic full-potential Korringa–Kohn–Rostoker total-energy method and applications *Phys. Rev.* B **54** 11187–98, available from: http://link.aps.org/abstract/PRB/v54/p11187
[47] Alexandre R, Rocha V M G S, Bailey S W, Lambert C J, Ferrer J and Sanvito S 2005 Towards molecular spintronics *Nat. Mater.* **4** 335–9, available from: http://www.nature.com/nmat/journal/v4/n4/full/nmat1349.html